Wave-equation migration of modelled elastic data

Richard A. Bale and Gary F. Margrave

ABSTRACT

Making use of elastic wavefield extrapolators to downward continue shots and receivers through layered isotropic or HTI media, we have developed a prestack shot-record elastic migration algorithm. The imaging conditions used are briefly explained, and the migration operators illustrated by impulse responses. Application of the algorithm to modelled isotropic data demonstrates the imaging of a density anomaly in an otherwise laterally invariant medium. The resolution of the P-SV image is superior to that of the P-P, as anticipated. Moreover, the illumination characteristics of the P-SV shot migrations differ in a complementary way to those of the P-P migrations. In future we anticipate extending the algorithm to laterally heterogeneous isotropic and HTI media.

INTRODUCTION

In Bale and Margrave (2003a) we describe elastic wavefield extrapolation for anisotropic media with HTI symmetry. In this paper we demonstrate the application of the elastic wavefield extrapolators in the context of prestack shot-record migration. The data used for this demonstration has been generated using the elastic pseudospectral modelling described in Bale (2002).

Previous work on elastic wave-equation migration includes: Etgen (1988), who used a Stolt algorithm on isotropic 2-D elastic data; Zhe and Greenhalgh (1997), who used a Helmholtz decomposition on isotropic data, combined with a split-step algorithm (Stoffa et al., 1990); and Hou and Marfurt (2003), who migrate all components with P- and S-velocities, and then separate modes within the imaging condition. Our algorithm differs from these in that we address explicitly the problem of migration in HTI media, where the shear-wave behaviour is complicated due to shear-wave splitting. Our wavefield extrapolators are therefore derived from the Kelvin-Christoffel equation (Bale and Margrave, 2003a) rather than using the standard Helmholtz decomposition, which only applies to isotropic media. Nonetheless, our algorithm is, of course, applicable to isotropic media, as is the case for the results presented here on modelled data.

In the next section we describe the algorithm, which is based upon elastic wavefield extrapolation combined with an appropriate set of imaging conditions. The migration impulse responses are shown for a few representative cases. In the following section we give the example using isotropic modelled data. We briefly discuss some observations based on the migration results. In the final section we draw some preliminary conclusions, and outline the direction of future work.

ELASTIC WAVE-EQUATION MIGRATION

Wave-equation migration fundamentally consists of two steps, wavefield extrapolation and imaging. Of these, wavefield extrapolation is the most demanding, both theoretically and computationally. The elastic wavefield extrapolation method we use is fully

described in a separate paper (Bale and Margrave, 2003a). Here we briefly describe the imaging conditions for elastic data.

Elastic imaging conditions

Shot record migration consists of (forward) extrapolating the shot downward, (backward) extrapolating the receiver wavefield downward to the same depth levels, and applying an imaging condition at each depth to obtain the migrated data. During elastic wavefield extrapolation the displacement wavefield is decomposed into three wave-modes P, S1 and S2, in each layer. For the forward extrapolation of the downgoing wavefield from the source, these are given by the vector of wave-mode amplitudes

$$\mathbf{w}_D = \begin{pmatrix} w_P^D & w_{S1}^D & w_{S2}^D \end{pmatrix}, \tag{1}$$

and, for backward extrapolation of the upgoing wavefield from the receiver, by the wave-mode vector

$$\mathbf{v}_U = \begin{pmatrix} v_P^U & v_{S1}^U & v_{S2}^U \end{pmatrix}, \tag{2}$$

Extrapolation of $\mathbf{w}_D$ and $\mathbf{v}_U$ from one layer to the next consists of applying a diagonal phase shift matrix to both vectors, and two different "interface propagators", $\mathbf{W}_{DD}$ and $\mathbf{W}_{UU}$ respectively, which are 3-by-3 matrices. Application of an interface propagator is equivalent to recomposing the displacement wavefields just above each interface and decomposing just below. The matrices $\mathbf{W}_{DD}$ and $\mathbf{W}_{UU}$ are the submatrices of the general 6-by-6 two-way propagator matrix (Fryer and Frazer, 1984), and are associated with one-way propagation only.

The goal of elastic migration, assuming a P-wave source, is to obtain images corresponding to P-P reflectivity, and P-S reflectivity for the isotropic case, or P-S1 and P-S2 reflectivity for the HTI case. Additional images such as S1-S2 can also be obtained if the source generates shear energy. To obtain these images we apply correlation imaging conditions between the corresponding elements of equations (1) and (2)

$$I_{MN}(x,z) = \int_0^{\omega_{\max}} \overline{w}_M^D(x,z,\omega) v_N^U(x,z,\omega) d\omega \tag{3}$$

where I_{MN} is the image for down-going mode M, and up-going mode N, where $M, N \in \{P, S1, S2\}$. The overscore denotes complex conjugation. Alternative imaging conditions, such as a deconvolution imaging condition, can of course be substituted.

Impulse responses

Figure 1 shows the finite (500 m) offset P-P and P-SV impulse responses in a homogeneous isotropic medium for vertical-displacement source and receivers, assuming a stress-free boundary. Figure 2 shows corresponding P-P and P-SV impulse responses for an HTI medium, with the symmetry axis lying in the plane of propagation (x-

direction). Figure 3 shows the P-S1 and P-S2 impulse responses for the same HTI medium, but when the symmetry axis lies at 45° to the x-direction.

EXAMPLES

We now demonstrate application of the elastic wave-equation migration algorithm on 2-D data which has been modelled using the pseudospectral method (Bale, 2002). The model (Figure 4) is isotropic, with velocity which depends only on depth. The low velocity at the bottom of the model is in fact part of an absorbing layer, used to suppress energy which wraps around from the top during pseudospectral modelling – the interface at the bottom is embedded within the absorbing layer, and does not contribute a reflection. The density anomaly is used to test the lateral focusing of the migration algorithm, whilst still using a laterally invariant velocity.

Figure 5 shows a shot record from the middle of the profile, above the circular anomaly. The shot is modelled as a P-wave explosive source, with X- and Z-displacements in (a), and up-going P and SV modes after wavefield decomposition in (b). The reflections from the two horizontal interfaces, as well as from the density anomaly are clearly seen.

In Figure 6, we show the results of shot-record elastic wave-equation migration applied to the modelled data. The migrations from three individual shots at 2060 m, 2560 m and 3060 m are shown in (a), (b) and (c). As expected, the depth resolution of the converted P-SV image is superior to that of the P-P image, because the slower shear-wave velocity corresponds to higher wave-numbers for any particular part of the source spectrum.

Another interesting feature observed here is the different effect of illumination angles on the P-P and P-SV images, in particular for the off-center shots in (a) and (c). Whereas the density anomaly appears rotated *towards* the shot position for the P-P images, it appears rotated *away* from the shot positions for the P-SV images. The explanation for this apparent paradox lies in the amplitude variation with angle for P-SV conversions. For P-P reflections, we have high amplitude at normal incidence, corresponding to the part of the density anomaly which faces the shot position. This also lies within the aperture of the receiver array for the shots considered, and therefore contributes significantly towards the image amplitude. For the P-SV case, the situation is more complicated. There is no reflection amplitude at normal incidence. Maximum conversion amplitude corresponds to angles around plus and minus 30° (this has not been computed for this specific case, but is typical for converted waves). Energy reflected with these angles will contribute when they are reflected towards the center of the profile, so that the energy falls within the receiver array, but not when they are reflected to the outsides of the model, beyond the receiver array. As a result, the strongest amplitude appears to be rotated away from the shot in the direction of the receiver array. In Figure (d) the image is formed from the migration of five shot records with lateral shot-positions ranging between 1560 m and 3560 m. The illumination from different angles provides a more complete imaging of the circular anomaly on both P-P and P-SV sections.

CONCLUSIONS AND FUTURE WORK

Elastic wavefield extrapolators have been incorporated into a shot-record migration scheme, using imaging conditions for different mode combinations. The code is applicable to both isotropic and HTI media, but is currently restricted to vertically heterogeneous velocities only. We have, to date, applied the migration to modelled data for an isotropic model with laterally invariant velocities, but with a circular density anomaly to test the lateral focusing. The results shown here suggest that elastic wave-equation migration properly images both P-P and P-SV data. Our results also indicate that the P-SV image offers advantages in resolution, as expected, and that the P-SV image may complement the P-P image from an illumination angle "point of view".

The full migration algorithm is yet to be applied to data from an HTI model, though the elastic wavefield extrapolators *have* been successfully tested on HTI modelled data. Furthermore we plan to extend the algorithm to handle lateral velocity (and anisotropy) variations, using the PSPI and NSPS algorithms (Margrave and Ferguson, 1999). Elastic extrapolators employing these techniques are currently being investigated (see Bale and Margrave, 2003b). Our eventual goal is to demonstrate imaging of P-S1 and P-S2 data in a model with heterogeneous HTI media, such as is frequently the case for fractured reservoirs.

ACKNOWLEDGEMENTS

The authors would like to acknowledge the support of sponsors of the CREWES project and of the POTSI project, towards this work.

The authors also thank Rob Stewart for helpful and illuminating discussions related to this work.

REFERENCES

Bale, R. A., 2002, Modelling 3D anisotropic elastic data using the pseudospectral approach: CREWES Research Report, **14.**

Bale, R.A. and Margrave, G.F., 2003b, Adapting elastic wavefield extrapolation to laterally varying HTI media: CREWES Research Report, Vol. **15**, this volume.

Bale, R.A. and Margrave, G.F., 2003a, Elastic wavefield extrapolation in HTI media: CREWES Research Report, Vol. **15**, this volume.

Etgen, J.T., 1988, Prestacked migration of P and Sv-waves, 58th Ann. Internat. Mtg: Soc. of Expl. Geophys., Session: S12.4.

Fryer, G.J. and Frazer, L.N., 1984, Seismic waves in stratified anisotropic media: Geophys. J. Roy. Astr. Soc., **78**, 691-710.

Hou A. and Marfurt, K., 2002, Multicomponent prestack depth migration by scalar wavefield extrapolation: Geophysics, **67**, 1886-1894.

Margrave, G.F. and Ferguson, R.J., 1999, Wavefield extrapolation by nonstationary phase shift: Geophysics, **64**, 1067-1078.

Stoffa, P.L., Fokkema, J.T., de Luna Freire, R.M., and Kessinger, W.P., 1990, Split-step Fourier migration: Geophysics, **55**, 410–421.

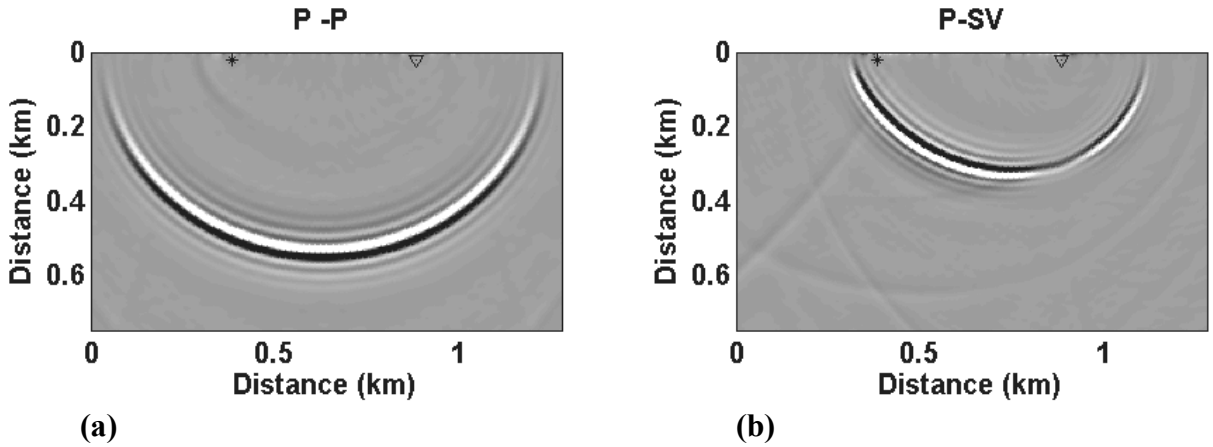

FIG. 1. Impulse responses in isotropic medium, with v_P=3000m/s, v_S=1500m/s, for vertical-displacement source and receivers, and stress-free boundary condition, showing: (a) P-P response and; (b) P-SV response. Source positions are indicated by "∗" and receivers by "▽", with a 500 m source-receiver offset.

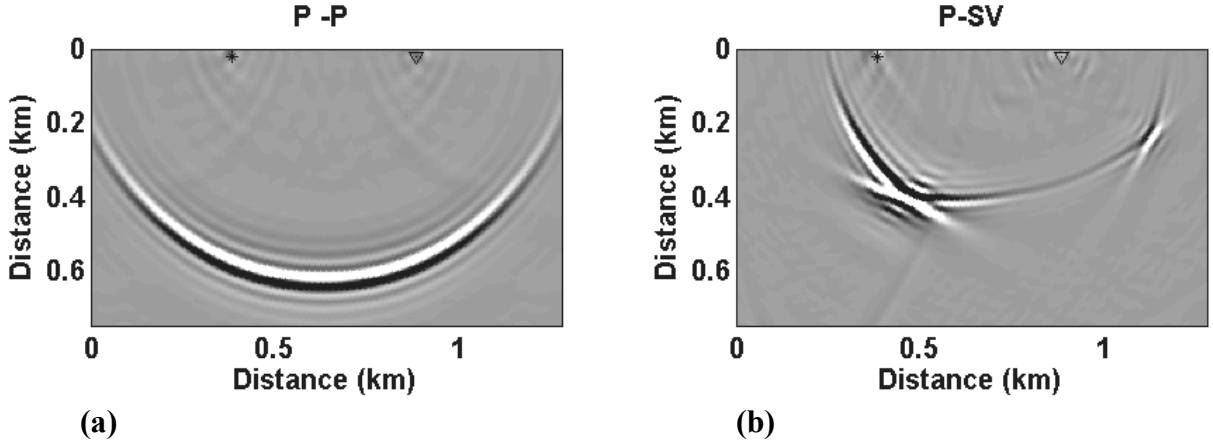

FIG. 2. Impulse responses in HTI medium, symmetry axis aligned with x-direction, for vertical-displacement source and receivers, showing: (a) P-P response and; (b) P-SV response. Compare with isotropic response in Figure 1.

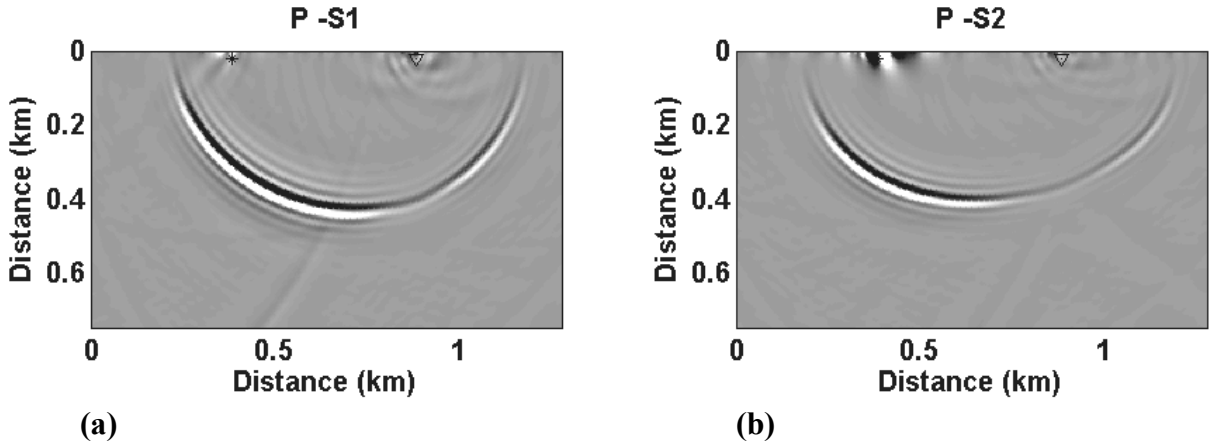

FIG. 3. Impulse responses in HTI medium, symmetry axis at 45° to x-direction, for vertical-displacement source and receivers.

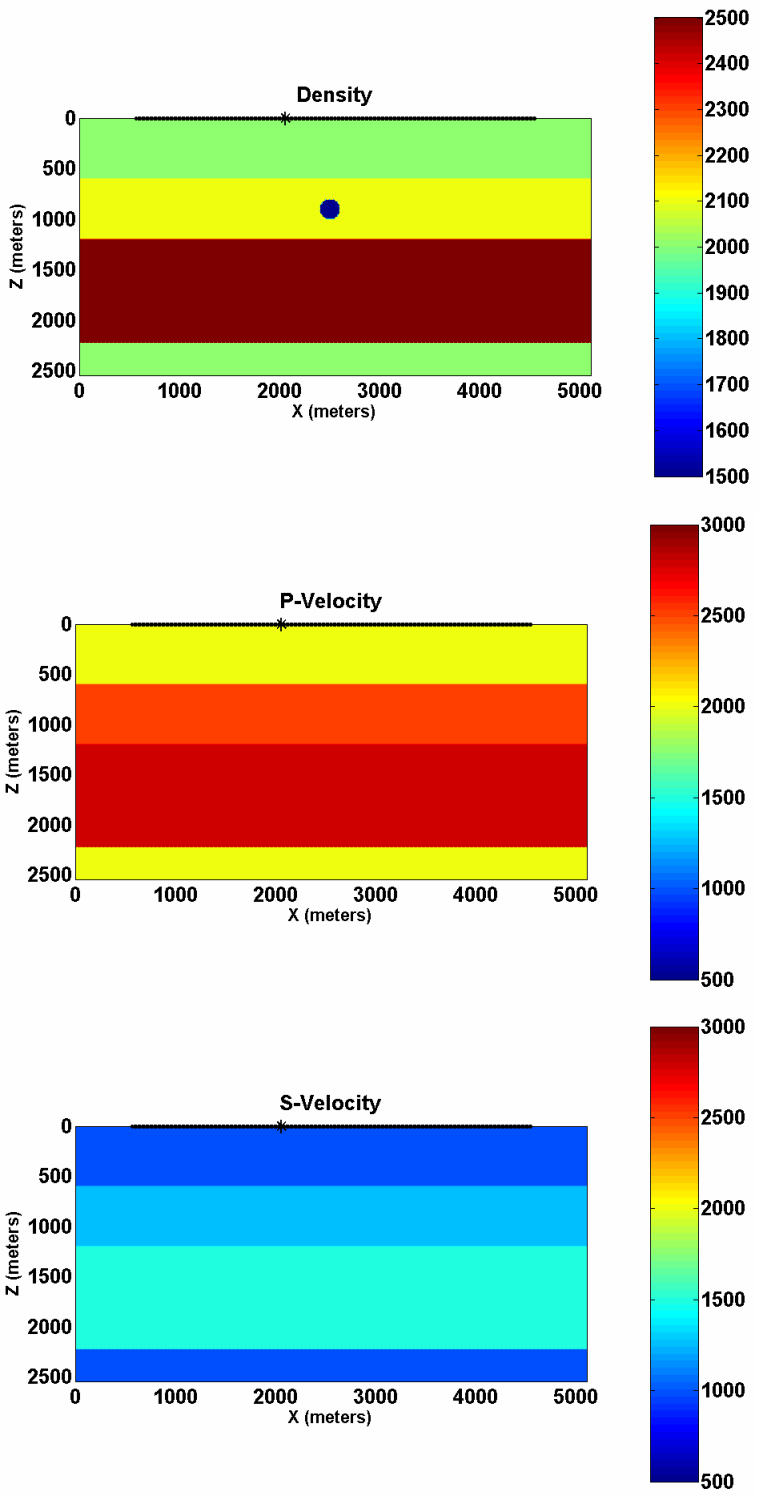

FIG. 4. Isotropic V(z) model for migration example.

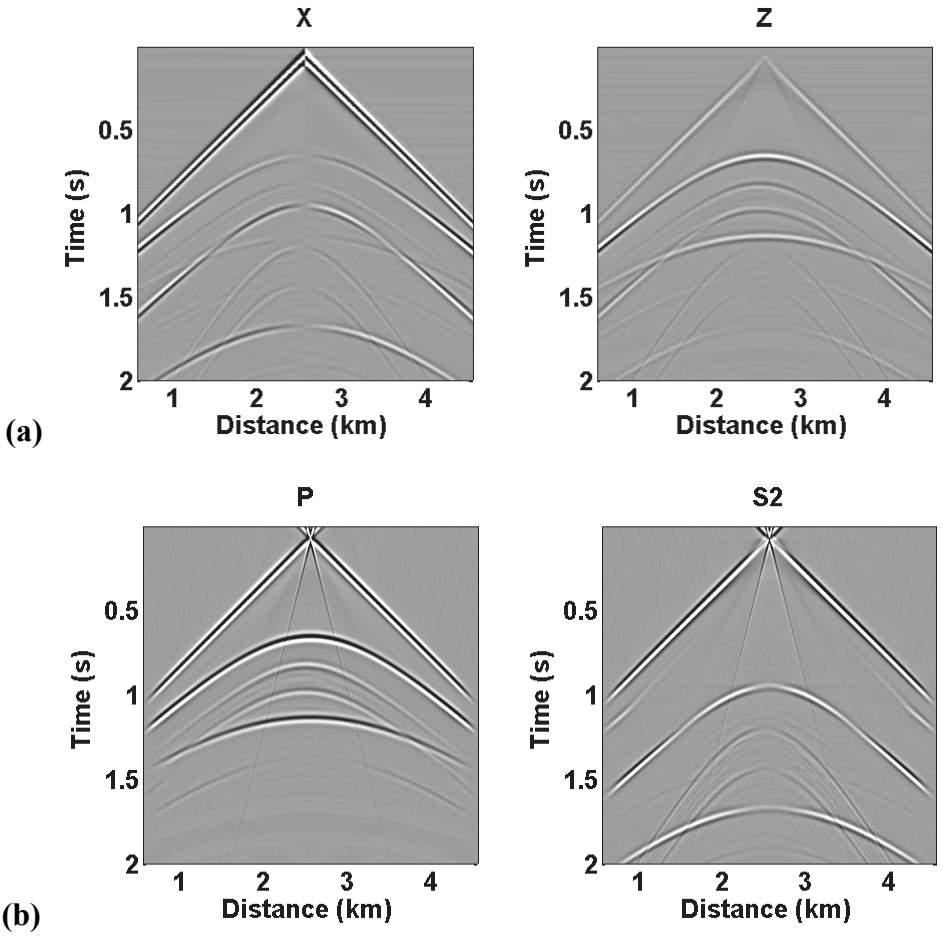

FIG. 5. Pseudospectral modelled shot-record for shot position 2560 m, using model of Figure 4. The X- and Z-components are shown in (a). The P- and SV-wave data after wavefield separation, are shown in (b). Two diffractions arising from the density anomaly are visible on the P-wave record at about 1 second, and on the SV-wave data at about 1.5 seconds.

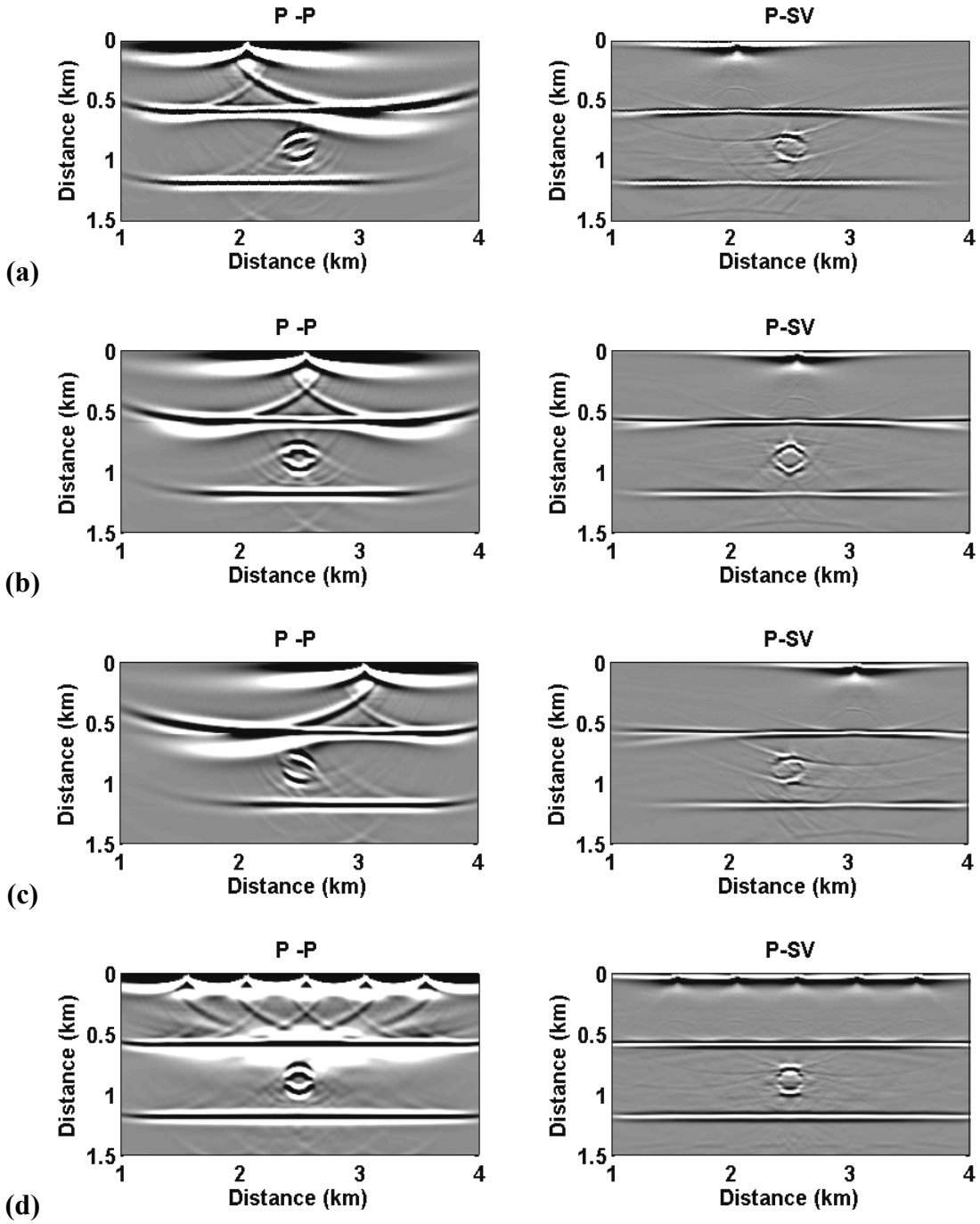

FIG. 6. Shot-record migrations for shots at: (a) x=2060 m; (b) 2560 m (the shot-record shown in Figure 5); and (c) 3060 m. P-P image on left, and P-SV (annotated as P-S2) on right. (d) Migration stack using five shots from 2560 m to 3560 m.